

Figure S1. Spatial distributions of genetic and viral expression in SNr, related to Figure 1.

(A) Representative overlay image of *in situ* hybridization against Slc32a1 (green), Pvalb (red), and TH (purple) mRNA in SNr and surrounding structures and zoom in on (A2) dorsolateral and (A3) ventromedial SNr domains. Neurons that are Slc32a1+ and Pvalb- are demarcated by white arrows in SNr and green arrows in SNC. (A4) Pvalb channel alone demonstrates (A5) strong expression in dorsolateral and (A6) weaker expression in ventromedial SNr.

(B) Density of neurons expressing Slc32a1 (green), Pvalb (black), and TH (grey) mRNA across rostral-caudal SNr sections (25 sections, 4 mice, 10,723 cells).

(C) Left: Representative overlay image and individual channels of *in situ* hybridization against Slc32a1 (green), Pvalb (red), and GAD2 (blue) mRNA in SNr and surrounding structures. Right: Quantification of gene co-expression in SNr GABAergic neurons and proportion of TH mRNA neurons in SNr. Across SNr, $84.0 \pm 0.2\%$ of Slc32a1-expressing GABAergic neurons expressed Pvalb and GAD2; $12.6 \pm 0.2\%$

expressed GAD2 and not Pvalb; 2.6 ± 0.01% expressed Pvalb and not GAD2; <1% were negative for Pvalb and GAD2 (14 sections, 3 mice, 4,178 cells).

(D) Left: Representative overlay image of within-section control for *in situ* labeling. Slc32a1 and Pvalb mRNA expression in the dentate gyrus of the hippocampus. Right: Quantification of Pvalb mRNA expression in Slc32a1+ neurons in the dentate gyrus (26.2 ± 0.01 %, 37 sections, 4 animals, 3,754 cells).

(E) 3D reconstructions of AAV injection sites in SNr for anterograde tracing. Each reconstruction shows an individual experimental animal aligned to an average SNr and projected in coronal view.

(F) Section stacks of aligned AAV injection sites in SNr, from rostral to caudal. Green= cells labeled in VGAT-Cre experiments, purple= cells labeled in PV-Cre experiments.

Diencephalon

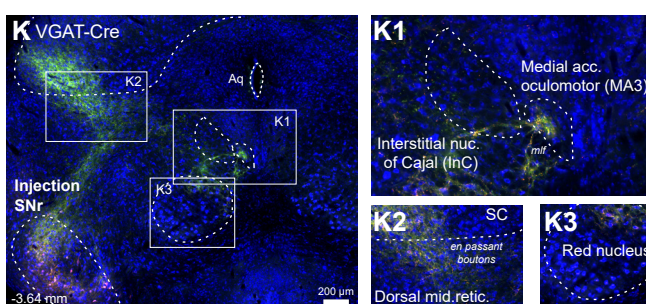
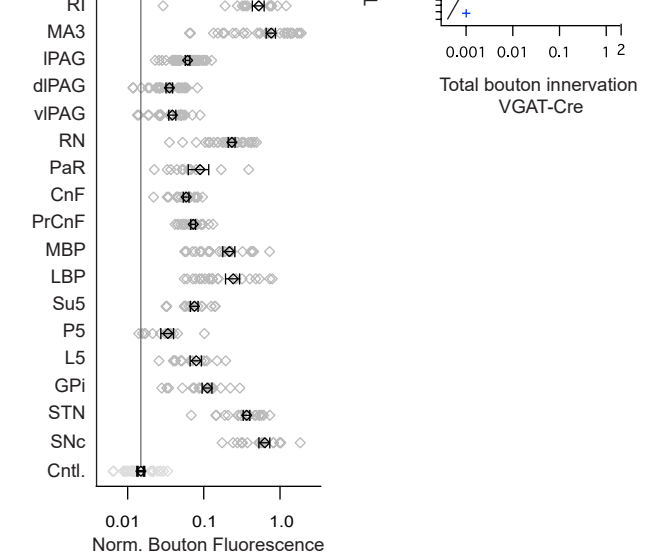
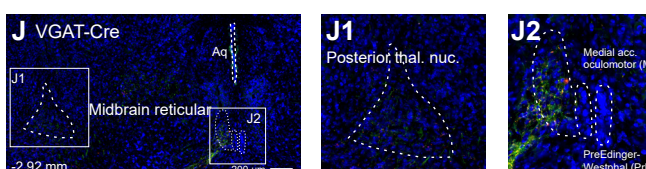
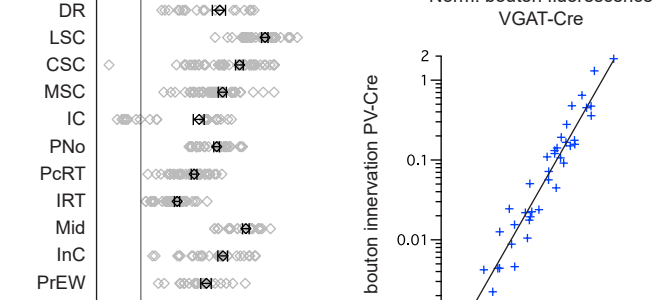
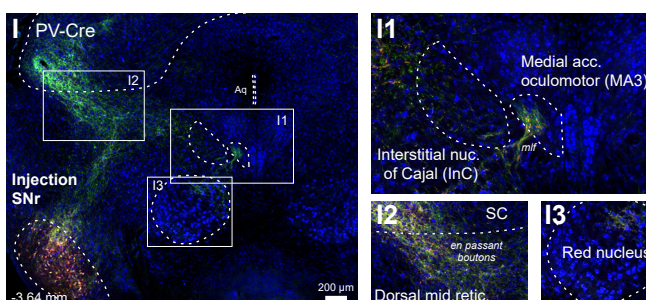
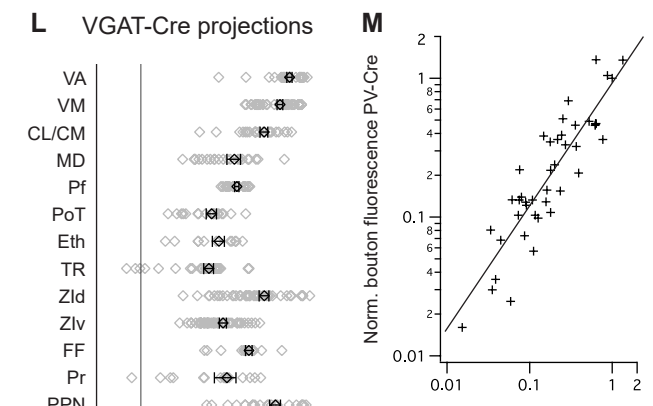
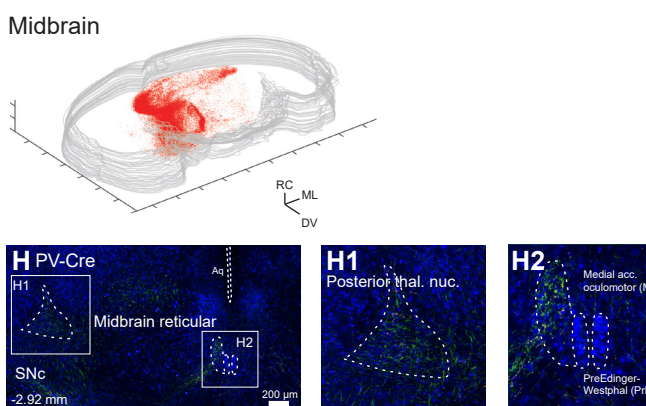
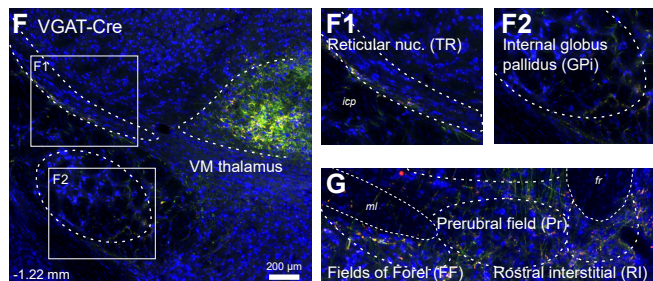
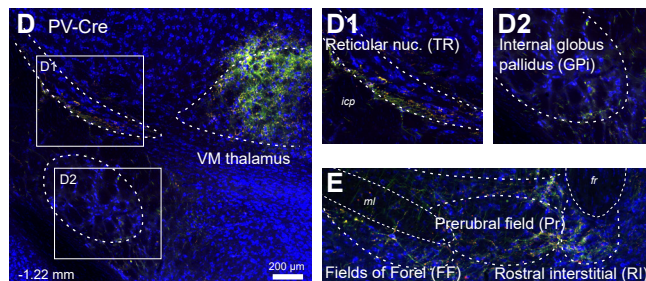
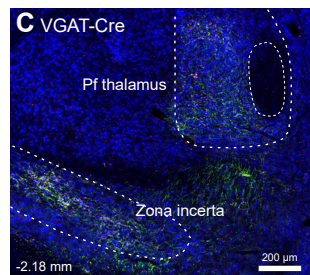
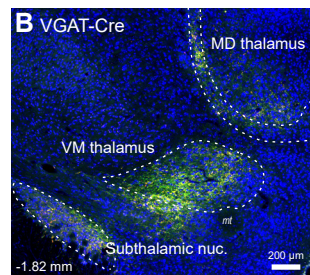
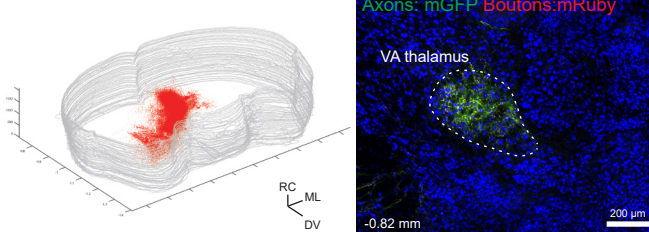


Figure S2. SNr innervation of nuclei in the diencephalon and brainstem, related to Figure 2.
AAV-DJ-hSyn-FLEX-mGFP-2A-Synaptophysin-mRuby injected into SNr of PV-Cre and VGAT-Cre mice labels SNr axons (green) and boutons (red).

(A-C) SNr projects to broad domains of the diencephalon. Dense innervation of VA and VM motor thalamus and relatively sparse innervation of MD and Pf thalamus, subthalamic nucleus and zona incerta in a VGAT-Cre mouse, comparable to that in PV-Cre (Figure 1).

(D-G) SNr bouton innervation of the thalamic reticular nucleus, internal segment of the globus pallidus, and subthalamic regions spanning the fields of Forel, prerubral field, and the rostral interstitial nucleus in (D, E) PV-Cre and (F, G) VGAT-Cre mice.

(H-K) Expanse of SNr terminal fields in the posterior thalamus and midbrain. Targets include (H1, J1) the posterior thalamic nucleus and small oculomotor structures, including (H2, J2) pre-Edinger-Westphal, (I1, K1) medial accessory oculomotor nuclei, and interstitial nucleus of Cajal. Additional innervation targets the (I3, K3) medial, dorsal red nucleus and (I2, K2) extensive en passant innervation spans large regions of the midbrain reticular formation, including regions immediately beneath the superior colliculus. Note: image histograms adjusted in each panel to best display axons and boutons.

(L) Quantification of bouton fluorescence in SNr targets labeled from injections in VGAT-Cre mice.

(M) Comparison of the SNr bouton intensity in each downstream region labeled in the VGAT-Cre and PV-Cre mice. (Top) Pairwise mean bouton fluorescence density per region. (Bottom) Total bouton fluorescence per region (arbitrary units).

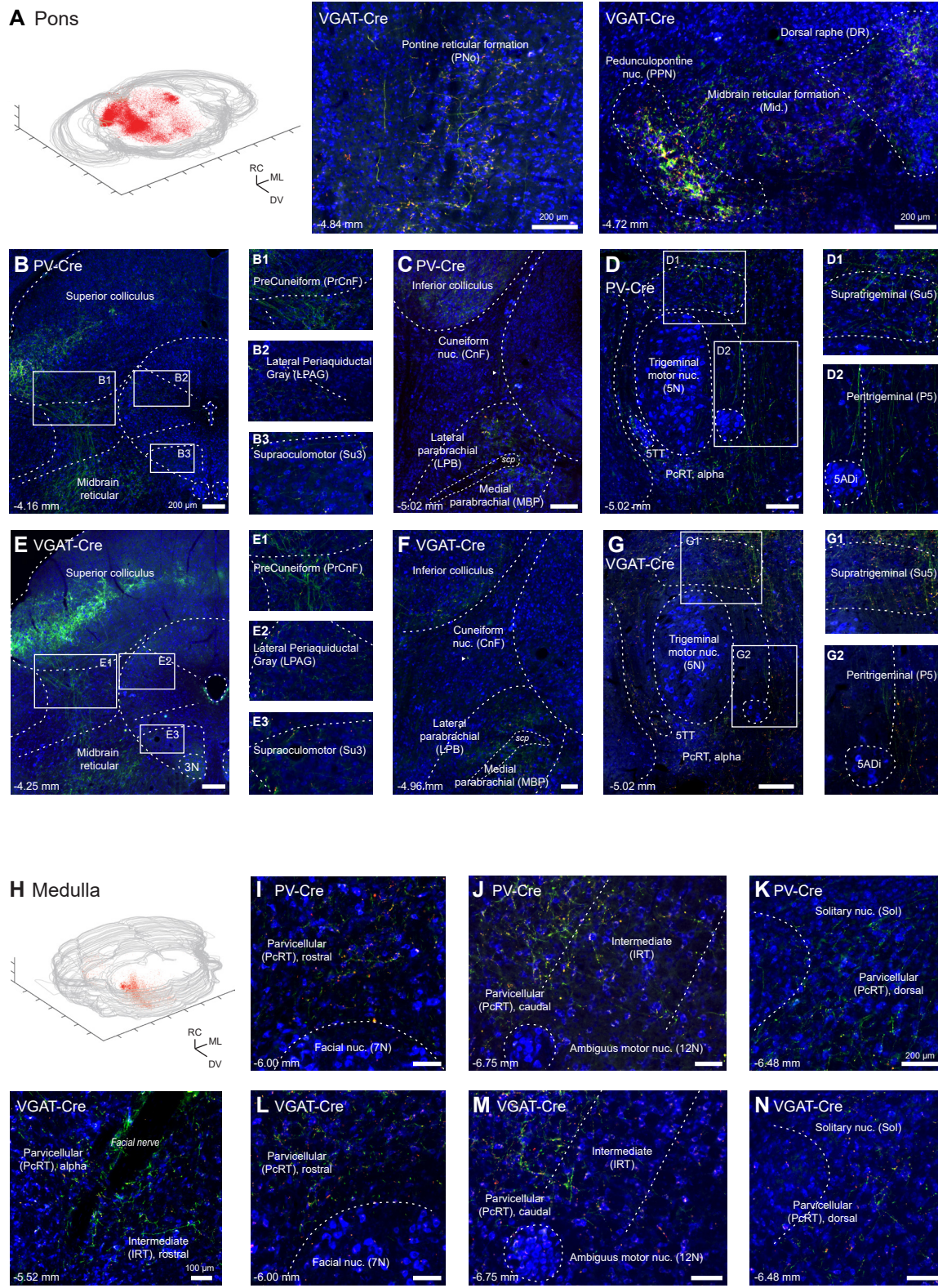


Figure S3. SNr innervation of diverse nuclei in the caudal brainstem, related to Figure 2.

(A) SNr bouton labeling spans large domains of the pons (left), including (middle) the PNo and (right) midbrain reticular formations, PPN, and dorsal raphe in a VGAT-Cre mouse, comparable to that in PV-Cre (Figure 1).

(B-G) SNr axons target diverse nuclei in the midbrain and pons, including robust innervation of the (B1, E1) precuneiform nucleus and only extremely sparse innervation of the (C, F) cuneiform nucleus of the mesencephalic locomotor region. Additional pontine targets include the (B2, E2) lateral periaqueductal grey, (B3, E3) sparse innervation of the supraoculomotor nucleus, and (C, F) denser innervation of the lateral and medial parabrachial nuclei. (D, G) SNr terminals also span nuclei surrounding the trigeminal motor nucleus, with putative en passant innervation of the supratrigeminal and peritrigeminal nuclei.

(H) Projections from SNr to the medulla span lateral portions of the medullary reticular formation (top) and nearby structures. (Bottom) Terminals are most dense in the parvicellular domain (PcRT) and extend into the neighboring intermediate domain (IRT) in the rostral medulla. SNr terminals span domains proximal to (I, L) facial (7N) and (J, M) ambiguus (12N) motor nuclei in the ventral medulla and (K, N) extend the full dorsal extent of PcRT. SNr terminals are scarcely found caudal of 12N.

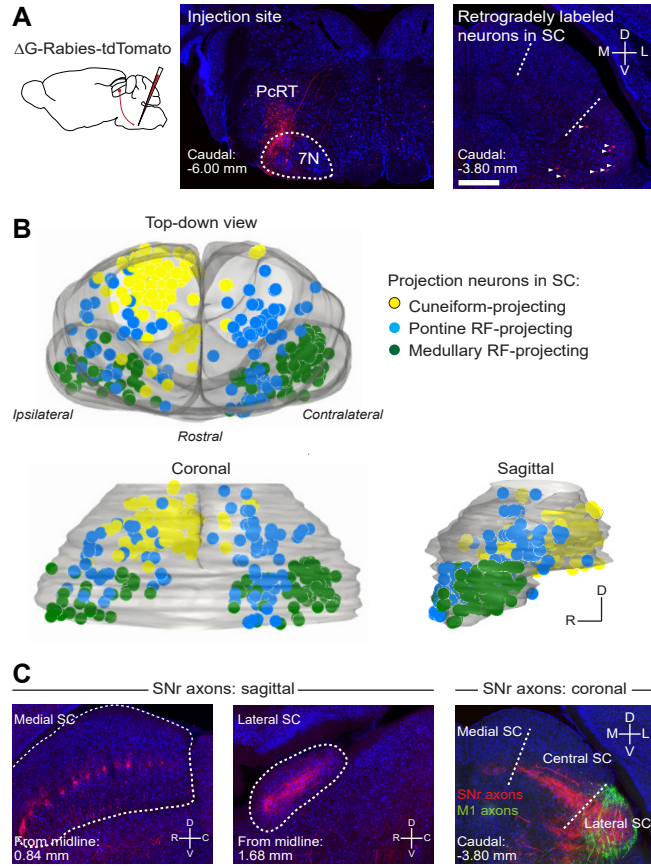


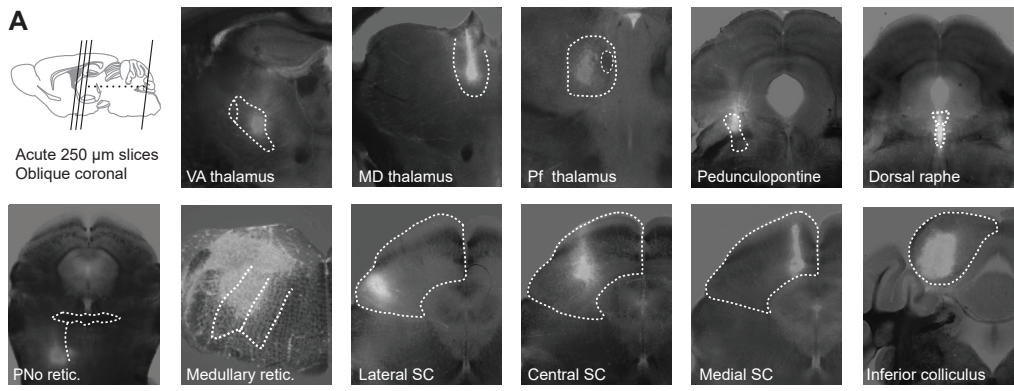
Figure S4. Topographical organization of efferents and afferents to the superior colliculus, related to Figure 4.

To map the spatial extent of superior colliculus projection domains in the mouse, retrograde and anterograde tracing delineates medial, central, and lateral subdivision coordinates.

(A) (Left) G-deleted rabies virus expressing tdTomato was injected into downstream regions to retrogradely label projection neurons. (Center) Example rabies injection site in the medullary reticular formation and facial motor nucleus (7N) in the medulla. (Right) Retrogradely labeled medulla-projecting neurons in the superior colliculus.

(B) Three-dimensional reconstructions of superior colliculus neurons projecting to the cuneiform nucleus (yellow), pontine reticular (blue), and medullary reticular (green) regions demonstrate a topographical bias of projection neurons, as observed in other species.

(C) AAV2.2-DIO-tdTomato injections into SNr of PV-Cre mice reveal SNr axons (red) extending across the superior colliculus. (Left) SNr axons form discrete, tufted clusters in medial and central domains of the superior colliculus, but (middle) SNr projections to lateral superior colliculus are diffuse. Note sections cut in sagittal plane. (Right) SNr projections to lateral superior colliculus overlap with projections from primary motor cortex (green), injected with AAV1-CamKII-eGFP.



B

Target	Animals	Caudal (mm)	Lateral (mm)	Ventral (mm)	Dextran Avg.(range)(nl)
Ventroanterior thalamus (VA)	5	0.80-0.82	1.00-1.10	3.60-3.70	108 (69-156)
Mediodorsal thalamus (MD)	3	1.16-1.22	0.40	3.10-3.30	83 (74-102)*
Parafascicular thalamus (Pf)	4	2.30-2.18	0.31-0.60	3.10-3.50	108 (83-133)*
Lateral superior colliculus (LSC)	6	3.52-3.80	1.25-1.50	2.25-2.50	138 (110-175)
Central superior colliculus (CSC)	5	3.52-3.97	0.75-1.25	2.10-2.25	138 (97-202)
Medial superior colliculus (MSC)	7	3.42-3.80	0.20-0.40	1.05-2.00	125 (97-152)*
Dorsal raphe (DR)	6	4.56-4.72	0.10-0.20	2.75-3.25	147 (133-156)*
Pedunculopontine (PPN)	4	4.36-4.96	1.20-1.35	2.50-3.75	165 (147-202)
Pontine reticular (PNo)	6	4.36-4.60	0.40-0.65	4.60	141 (73-181)
Inferior colliculus (IC)	4	4.80-5.21	1.35-1.43	2.30-2.75	130 (101-147)
Medullary reticular (Med)	6	5.80-6.84	0.75-1.75	5.00-5.60	265 (152-300)

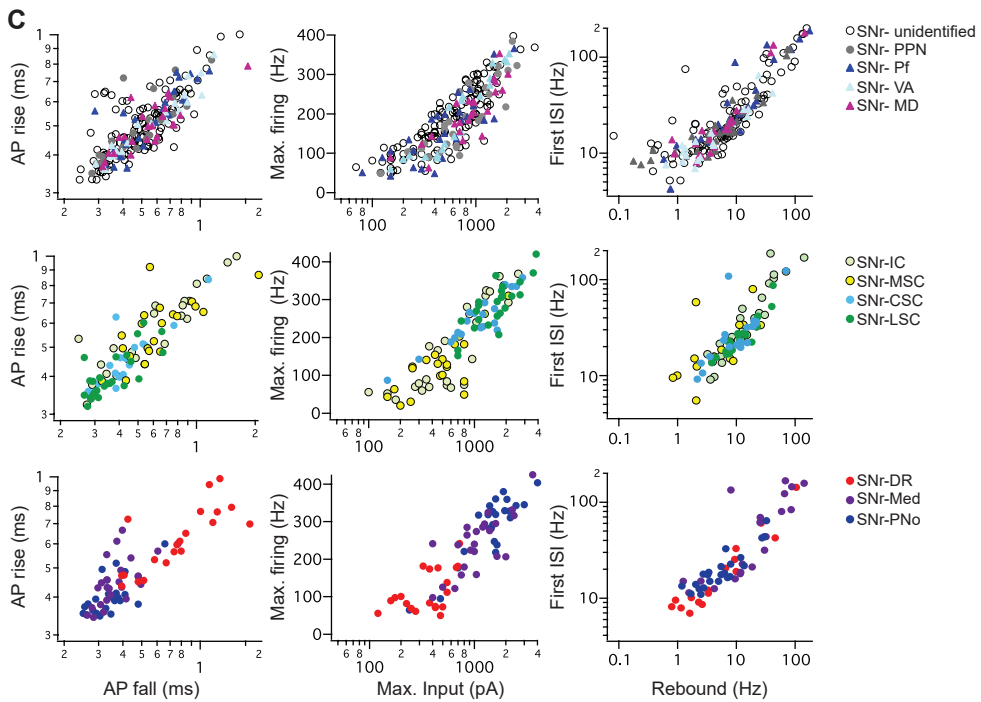


Figure S5. Injection parameters for retrograde labeling of SNr projection neurons for electrophysiological recordings, related to Figures 4 and 5.

(A) Representative injection sites of retrograde fluorescent dextran tracers. Oblique coronal sections fresh cut at 250 μm on a vibratome. Overlays of fluorescent and brightfield channels.

(B) Injection parameters for retrograde tracings from large SNr targets. Dextran volumes marked with an asterisk indicate targets alternatively injected with a solid tracer microinjector (see Methods).

(C) Comparison of additional electrophysiological features of retrogradely labeled SNr neurons.

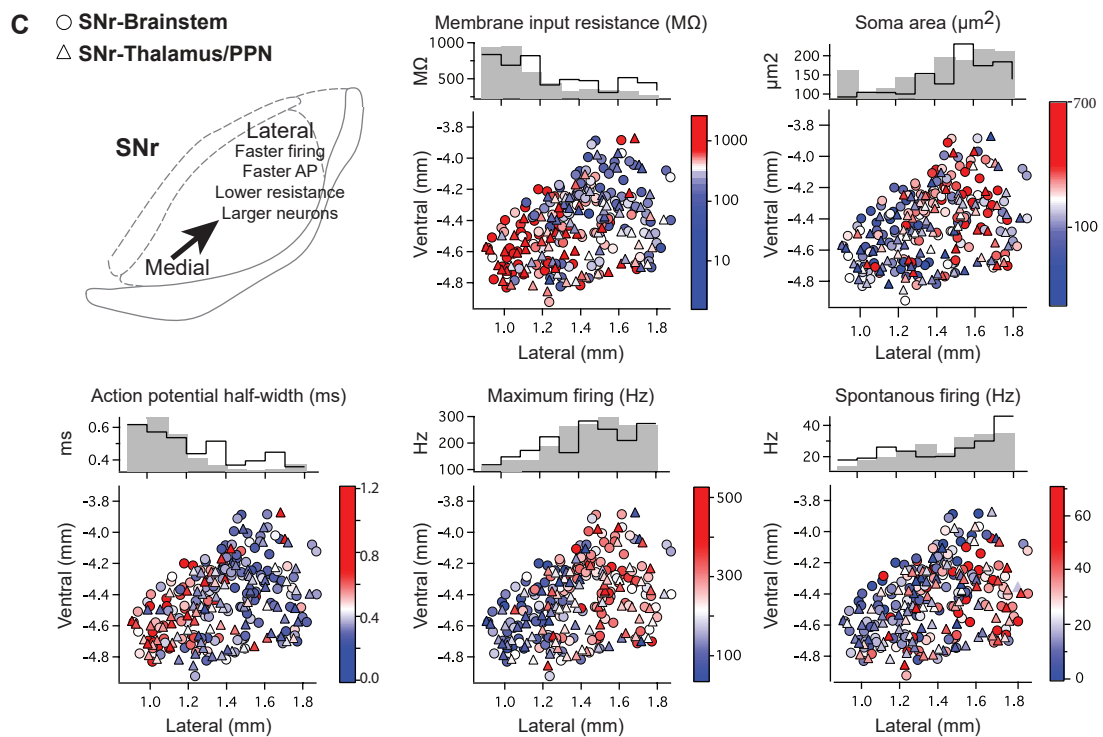
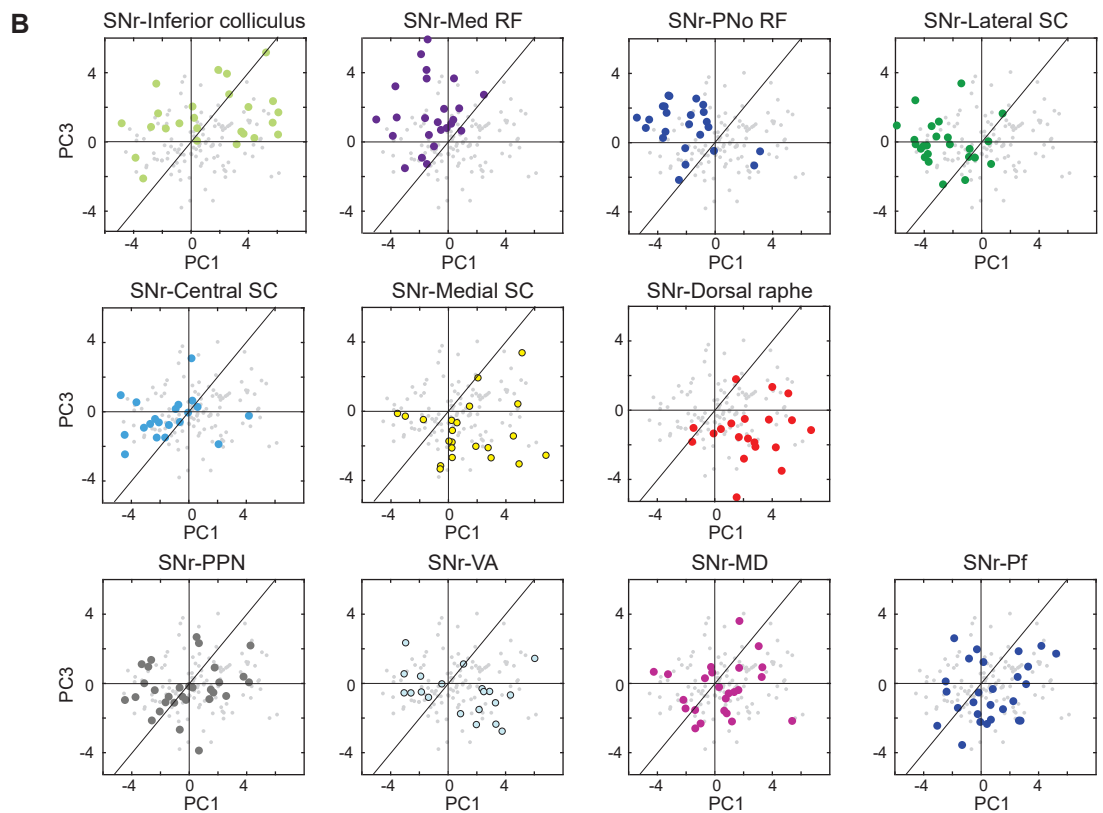
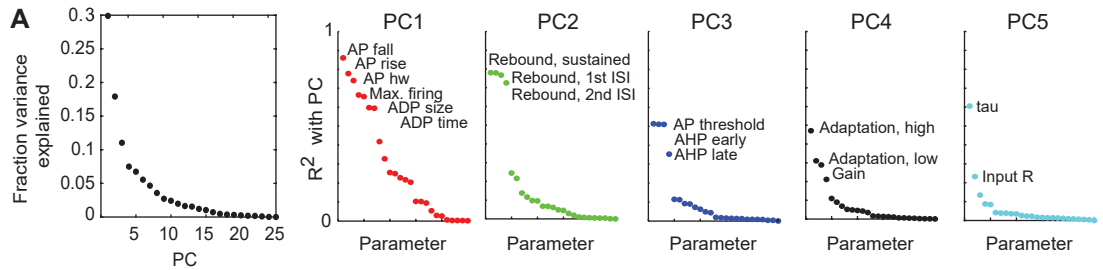
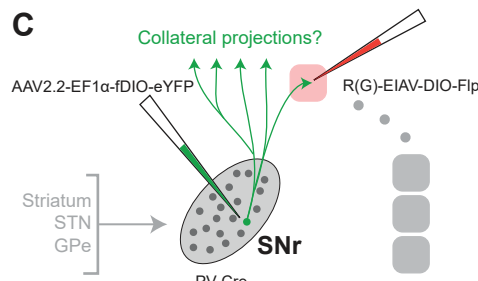
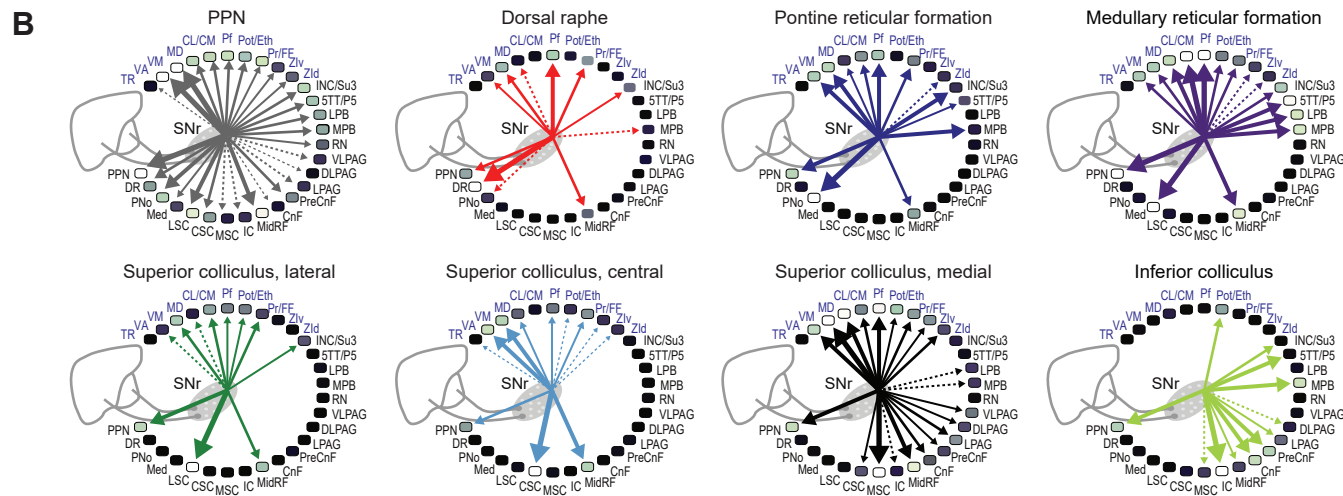
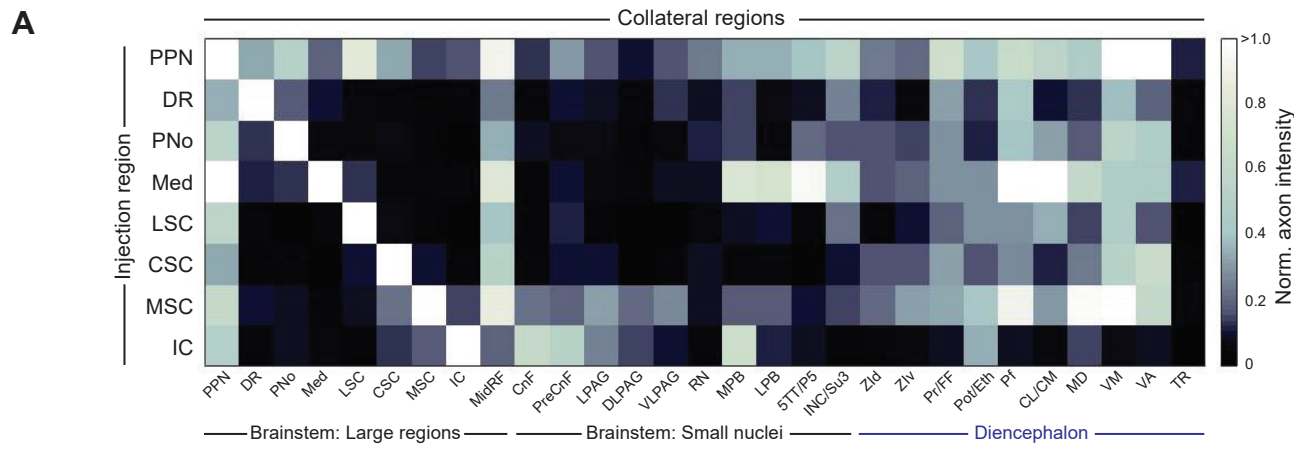


Figure S6. Intrinsic electrophysiological properties of SNr projection neurons and their spatial organization, related to Figures 4-5.

(A) Principal component analysis (PCA) of intrinsic properties in SNr (403 neurons) by singular value decomposition. (Left) Fraction of variance explained by each principal component. (Right) Correlations (R^2) of the first five principal components (PC1-PC5) with intrinsic property parameters. PC1 is highly correlated with fast spiking parameters, PC2 with post-inhibitory rebound parameters, PC3 with slow spiking parameters, P4 with parameters related to sustained firing, and PC5 with membrane properties.

(B) Plots of principal components PC3 versus PC1 for labeled SNr projection populations. Neurons retrogradely labeled from each identified downstream target (color coded) and randomly targeted SNr neurons (small grey points).

(C) Spatial organization of electrophysiological and morphological properties across SNr. Composite of recording locations of all SNr neurons retrogradely labeled from the thalamus/PPN (triangles, from Figure 5) and seven large brainstem domains (open circles, from Figure 4). In each plot, each recorded neuron is colored according to the heatmap of the values of the labeled electrophysiological property. Neuron location axes in coordinates lateral (x) and ventral (y) to Bregma, across all rostral-caudal levels of SNr. Bar graphs of property values projected onto the x-axis display medial-lateral distributions of neurons projecting to thalamus/PPN (black lines) and to large brainstem domains (grey bars).



D R(G)-EIAV-DIO-Flp in LSC
AAV2.2-EF1 α -fDIO-eYFP in SNr

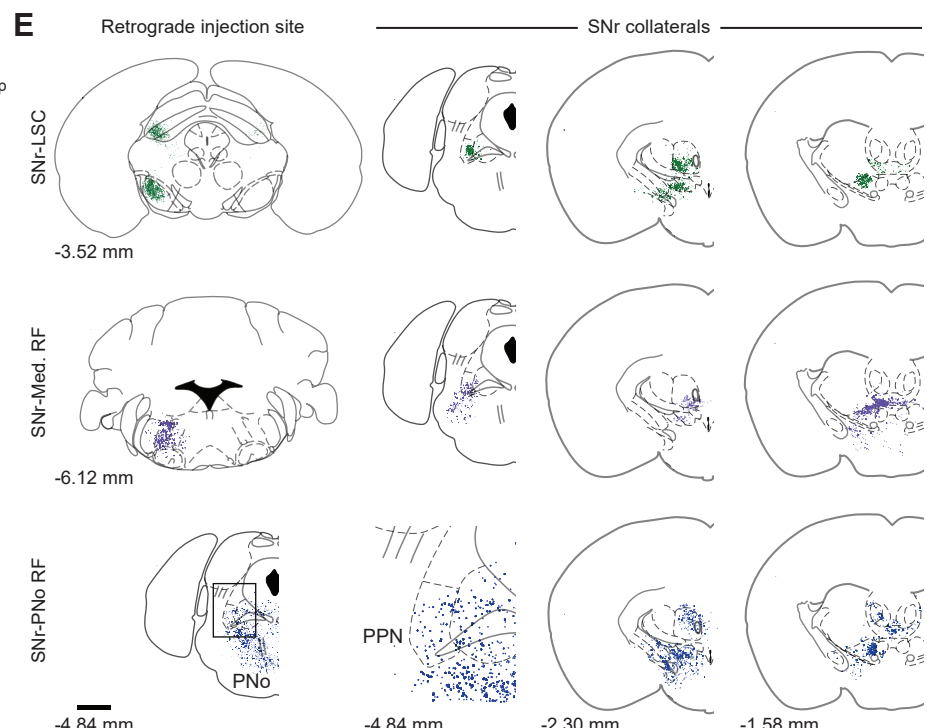
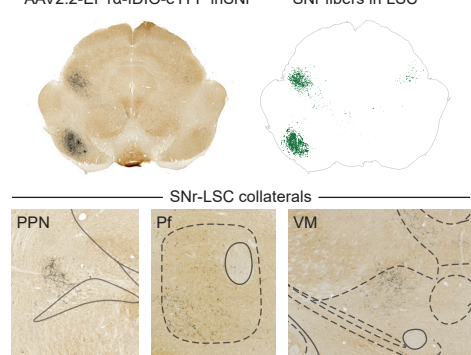


Figure S7. Collateral connections from SNr projection populations, related to Figure 6.

(A) Heatmap of collateral projection strengths from different SNr projection populations. Normalized axon intensity across SNr targets (columns) following injection of a retrograde Cre-expressing lentivirus into one of eight large brainstem regions (rows) reveals the extensive, but specific, SNr axon collateralization distribution. Axon collateral intensity is normalized to the intensity in the lentivirus injection region in each experiment.

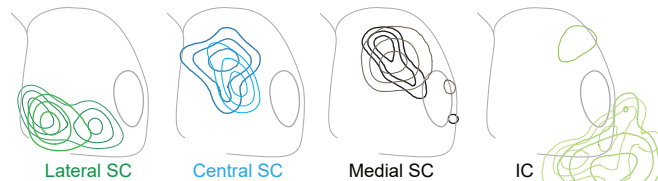
(B) Summary diagrams of SNr collateral projections. The target of the lentivirus injection is labeled above each summary diagram. The density of axonal collaterals from SNr to each target, normalized to the target of the lentivirus injection, is given by line thickness. Thickness binned according to decreasing ranges of >1.00, 1.00 - 0.51, 0.50 - 0.31, 0.30 - 0.21. Collateral axon density of 0.20 - 0.15 shown as dashed line.

(C) Schematic of genetic- and projection-based intersectional tracing strategy in which a retrograde virus expressing Cre-dependent Flp (RV(G)-EIAV-DIO-Flp) was targeted to a downstream region and a Flp-dependent AAV (AAV2.2-EF1a-fDIO-eYFP) was targeted to SNr in a PV-Cre mouse.

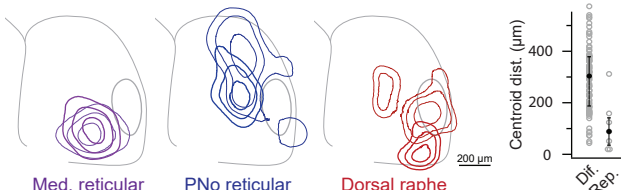
(D) (Top) Example section showing (left) eYFP+ dark-product neurons in SNr and axons in the lateral superior colliculus (LSC) following injection of RV(G)-EIAV-DIO-Flp into the LSC and AAV2.2-EF1a-fDIO-eYFP into SNr and (right) computationally segmented eYFP signal for easy visualization. (Bottom) Collateral terminals of SNr-to-LSC projection neurons are found in several regions, including the PPN, Pf thalamus, and VM thalamus.

(E) Comparison of SNr axon fields labeled via genetic- and projection-based intersectional collateral strategy. Distinct SNr projection populations targeted via RV(G)-EIAV-DIO-Flp injections to (top) LSC, (middle) medullary reticular formation, and (bottom) pontine (PNo) reticular formation. SNr axons labeled in (left column) targeted structures and (right) collateral axons in the PPN, Pf thalamus, and VM thalamus.

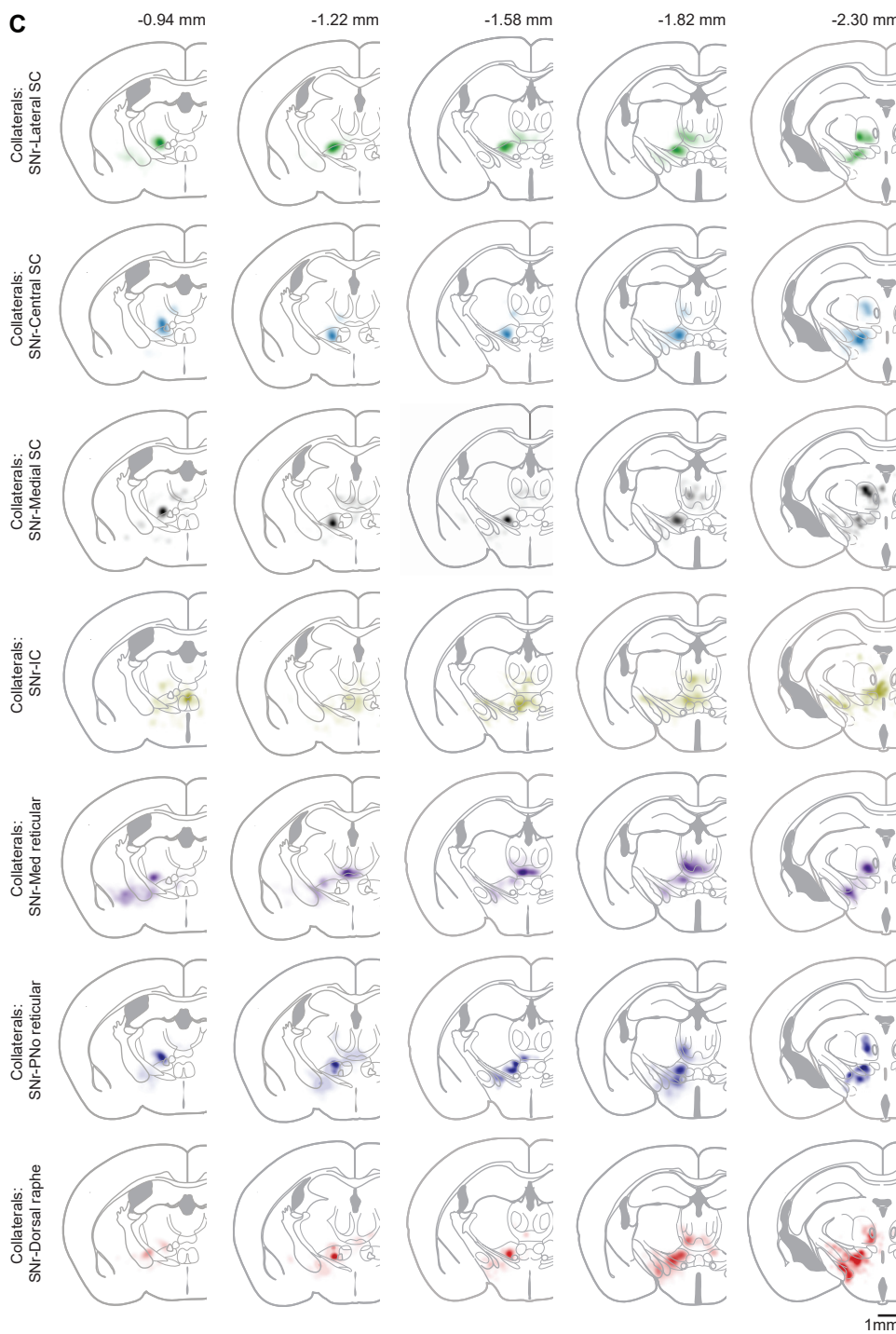
A SNr-to-colliculus collaterals: isodensity contour plots



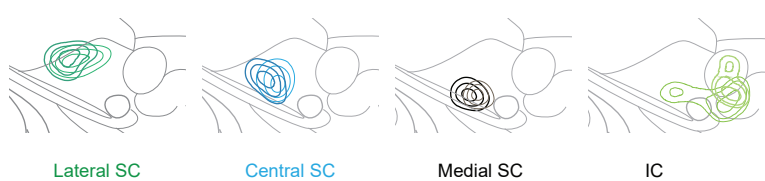
SNr-to-hindbrain collaterals: isodensity contour plots



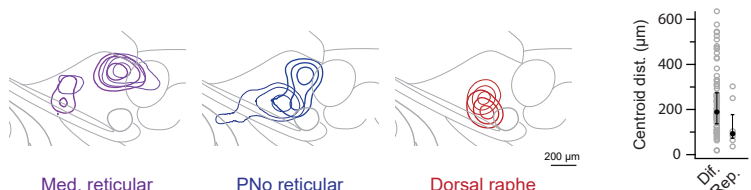
C



B Collaterals of SNr-to-colliculus: isodensity contour plots

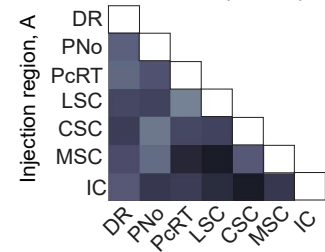


Collaterals of SNr-to-hindbrain: isodensity contour plots

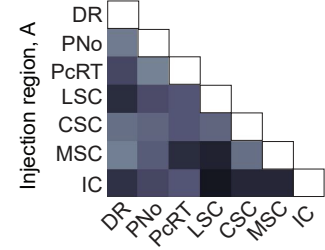


D

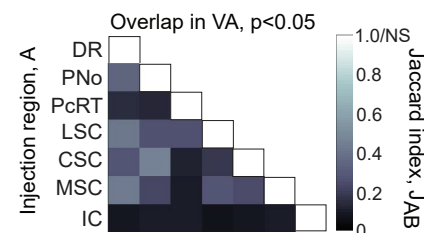
Collateral overlap in Pf, p<0.01



Overlap in VM, p<0.01



E



F

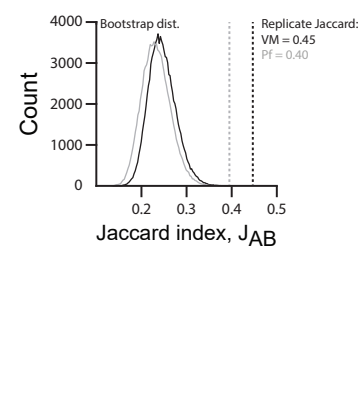


Figure S8. Topographical organization of ascending collateral projections from distinct SNr-subpopulations, related to Figure 7.

(A) Isodensity contour plots showing locations in Pf thalamus of SNr axon collaterals labeled from different brainstem regions (different colors) and replicate injections (thick vs. thin lines). Euclidean distances between centroid locations of axon terminal fields labeled from different and replicate brainstem injections (bottom right).

(B) Isodensity contour plots showing locations in VM thalamus of SNr axon collaterals labeled from different brainstem regions (different colors) and replicate injections (thick vs. thin lines). Euclidean distances between centroids of axon terminal fields labeled from different and replicate brainstem injections (bottom right).

(C) Heatmaps of axon collateralization density from SNr subpopulations retrogradely labeled from distinct brainstem regions (top-to-bottom) across rostral-caudal levels of thalamus (left-to-right). Serial sections aligned and stacked, centered at the corresponding sections in Paxinos and Franklin (2008). Data merged from replicates and heatmaps smoothed over 50 μ m intervals.

(D) Quantification of the overlap of SNr collateral axonal projections by the weighted Jaccard index. Index calculated for pairwise for collaterals of SNr-brainstem targets, labeled 'A' and 'B'. The intensity corresponds to the value of the Jaccard index J_{AB} . Statistical significance calculated via data shuffling. Note differences in VA are not highly significant.

(E) Comparison of J_{AB} across replicate experiments in Pf and VM versus the bootstrap estimate of the expected distribution of J_{AB} under the null hypothesis that targets lack spatial segregation, $p < 0.001$.